

Porosity characterization of fiber-reinforced ceramic matrix composite using synchrotron X-ray computed tomography^{*}

Chunrong Zou^{a*}, T. James Marrow^{b,c}, Christina Reinhard^d, Bin Li^a,
Changrui Zhang^a, and Siqing Wang^a

^a *Science and Technology on Advanced Ceramic fibres and Composites Laboratory, National University of Defense Technology, Changsha 410073, Hunan Province, PR China*

^b *Department of Materials, ^cOxford Martin School, University of Oxford, Parks Road, Oxford OX1 3PH, United Kingdom*

^d *Diamond Light Source, Harwell Science and Innovation Campus, United Kingdom*
E-mail: crzounudt@hotmail.com

ABSTRACT: The pore structure and porosity of a continuous fiber reinforced ceramic matrix composite has been characterized using high-resolution synchrotron X-ray computed tomography (XCT). Segmentation of the reconstructed tomograph images reveals different types of pores within the composite, the inter-fiber bundle open pores displaying a “node-bond” geometry, and the intra-fiber bundle isolated micropores showing a piping shape. The 3D morphology of the pores is resolved and each pore is labeled. The quantitative filtering of the pores measures a total porosity 8.9 % for the composite, amid which there is about 7.1~9.3 % closed micropores.

KEYWORDS: Fiber-reinforced composites; Porosity; X-ray computed tomography; segmentation; 3D morphology .

^{*} This is the authors' copy of a paper subsequently published as: C. Zou, T.J. Marrow, C. Reinhard, B. Li, C. Zhang, S. Wang, Porosity characterization of fiber-reinforced ceramic matrix composite using synchrotron X-ray computed tomography, *J. Instrum.* 11 (2016) C03052. doi:10.1088/1748-0221/11/03/C03052.

Contents

1. Introduction	1
2. Material	1
3. X-ray computed tomography and analysis	2
4. Results and discussion	2
4.1 Segmentation of pores	2
4.2 3D pore morphology and porosity analysis	4
5. Conclusions	6

1. Introduction

Continuous fiber reinforced ceramic matrix composites (FCMCs) are promising structural materials for high-temperature applications [1]. Polymer Impregnation Pyrolysis (PIP) method has been widely used in fabricating FCMCs, which has the advantages of low fabrication temperature, high purity and homogeneous ceramic matrix, and large-scale components fabrication [2]. However, the PIP densification process is usually incomplete, resulting in a relatively high residual porosity. The network of the pores could have a strong influence on the mechanical behaviour of the composite [3, 4]. Thus, it is necessary to have a comprehensive understanding on the pore structure and 3D morphology in addition to the porosity of the composites. The result can establish the relationship between the densification process and structural change of FCMCs, and provide real 3D pore morphology for microstructure based composite modeling [5].

Generally, the open porosity of a material can be measured by means of the Archimedes principle or mercury intrusion method, but the pore structure is not available by either method [6]. Two-dimensional techniques i.e. optical and electron microscopy are efficient for observing the pore structure. However, they demonstrate only limited information about the three-dimensional pore structure. In comparison, X-ray computed tomography (XCT) is a non-destructive technique that can reproduce the accurate 3D morphology of material by the reconstruction of a series of radiographic projections [7]. With sufficient resolution and the beneficial effects of phase contrast, XCT allows direct identification of the position, dimension and 3D shape of pores [8]. This paper assesses the feasibility of using XCT to characterize the volumetric porosity in FCMCs. The inter-fiber bundles open pores and intra-fiber bundle close pores are segmented and their 3D porosity morphology is visualized. The observed total porosity and closed porosity are then quantified.

2. Material

The 2.5D SiNO_f/BN composite was prepared by the PIP method using liquid borazine as the precursor for BN matrix. The SiNO fibers (National University of Defense Technology) were weaved into 2.5D SiNO fiber preform prior to composite fabrication, which had a fiber content

of approximately 41 vol.%. Liquid borazine was firstly infiltrated into the fiber preform though a vacuum assisted method. The infiltrated preform with residual precursor was then moved into an autoclave. Cross-linking and consolidation of the precursor was conducted at 90 °C, with an initial N₂ pressure of 3 MPa. Subsequently, the solid preform was pyrolysed at 1000 °C for 1h under N₂ atmosphere to produce 2.5D SiNO_f/BN composite. With three cycles of the above infiltration and pyrolysis process (the pyrolysis temperature of the last cycle was increased to 1200 °C), the final dense composite was obtained. The resulted density was about 1.85 g/cm³ and the open porosity was measured as 7.5 % by the Archimedes method [9].

3. X-ray computed tomography and analysis

The high-resolution synchrotron X-ray computed tomography experiment was performed at the Diamond Light Source (Oxfordshire, UK), Joint Engineering, Environmental and Processing beam line (I12-JEEP, external hut), using the PCO4000 camera and the Module 3 optics. The projections were obtained at an X-ray beam energy of 53 keV with a nominal voxel size of 1.9 μm. The sample to detector distance was approximately 250 mm. After reconstruction using back-filtered projection [10], the cropped Region of Interest (ROI) had a data size of 2080×2400×1600 voxel. The volumetric reconstruction of the specimen (ROI) and the corresponded coordinates are shown in Fig. 1a.

The tomography images were analysed using the Avizo Fire software (Visualization Sciences Group, Bordeaux, France). Before segmentation, 3D median image filtering was applied to reduce the noise of the data. By applying contrast thresholding, the inter bundle pores and intra-fiber bundle pores were identified and segmented. The pores were then binary-separated and labeled for porosity analysis.

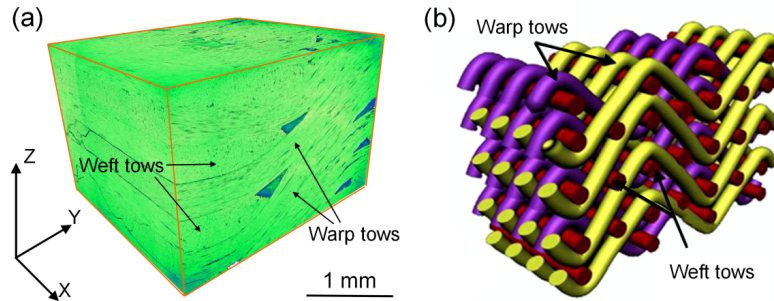


Fig. 1 (a) Reconstruction of the specimen of ROI; (b) Illustration of 2.5D fabric architecture^[11]

4. Results and discussion

4.1 Segmentation of pores

The 2.5 D fabric architecture contains curved warp fiber bundles across the plane of weft fiber bundles, which introduces desirable damage tolerance between adjacent fiber planes. By comparing Fig. 1a with Fig. 1b, the different warp and weft fiber bundles within the 2.5D SiNO_f/BN composite can be distinguished. However, the deformed warp fibers also generate complex pores that are difficult to be fully filled during densification. Such residual pores would suffer from stress concentration under load and lead to the failure of the composite. Fig. 2 shows the Ortho view images of the reconstructed specimen. Good image contrast has been

obtained and the different phases, fiber/matrix and pores, can be clearly distinguished. The reconstructed images reveal that the individual fiber bundles are well densified while certain large pores are present at the conjunction areas of different fiber bundles. Long through-pores along bundle interfaces are also visible. These inter-fiber bundle large pores and through-pores are defined as open pores.

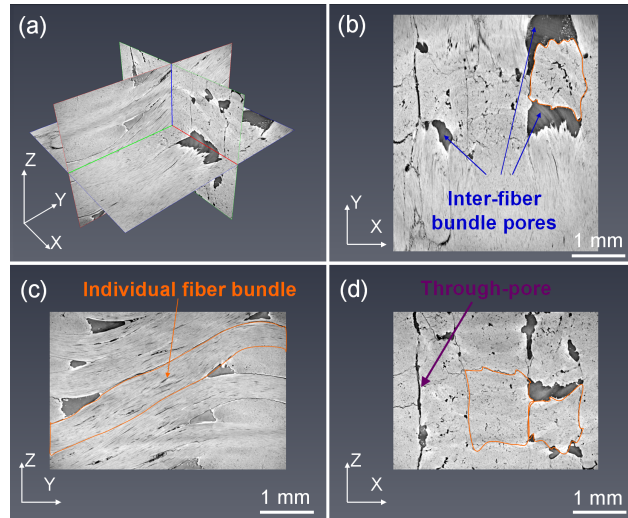


Fig. 2 Ortho view slices of the reconstructed specimen

By segmenting the open pores, as shown in Fig. 3a-c, connecting pore networks have been resolved. Such pore networks exhibit a “node-bond” geometry, that is large pores (named as nodes) at the intersection position are connected by the dendritic through-pores (named as bonds), as has been proposed by Starr [12]. The bonds are primary tunnels for liquid precursor to penetrate into the large nodes during densification. However, the bonds are tortuous and their paths narrow quickly as the PIP proceeds, leading to the decrease of infiltration efficiency. It would therefore need more time to further densify the large nodes. Once the bonds are fully blocked, further densification of the nodes becomes impossible, leaving large pores within the composite.

Beside the open pores, the X-ray in the present study also provides sufficient resolution to directly observe the close micropores within individual fiber bundles, which would normally be unavailable or be neglected by other conventional methods. As shown in Fig. 3d-f, the micropores tend to have a shape similar to piping and are mostly attached to the fiber axial. The diameter of the micropores varies from less than one fiber diameter to 2~3 times of fiber diameter (20~30 μm), while the length is up to 30~40 times of fiber diameter (300~400 μm). The distribution of these pores is relatively uniform, indicating the liquid precursor has a good wettability against the fibers and can penetrate effectively within the fiber bundles.

The inhomogeneous structure of the matrix, as well as the formation of different scaled pores is closely related to the PIP process of the composite. Generally, the deposition of matrix is easier within individual fiber bundles since the accessible surface area provided are much higher than that of the inter-fiber bundles [13]. Thus, it can be speculated that the individual fiber bundles could quickly reach their maximum density while retaining some isolated micropores. Meanwhile, the dense of the “node-bond” open pores would continue until the paths for liquid precursor become completely blocked. In addition, the formation of large pores could be affected by the high vapor pressure of liquid borazine at room temperature. During

vacuum infiltration, the vapor of borazine could have firstly occupied the large conjunction pores and inhibited their densification. The resultant matrix is characterised by dispersive and discrete, as shown in Fig. 3d.

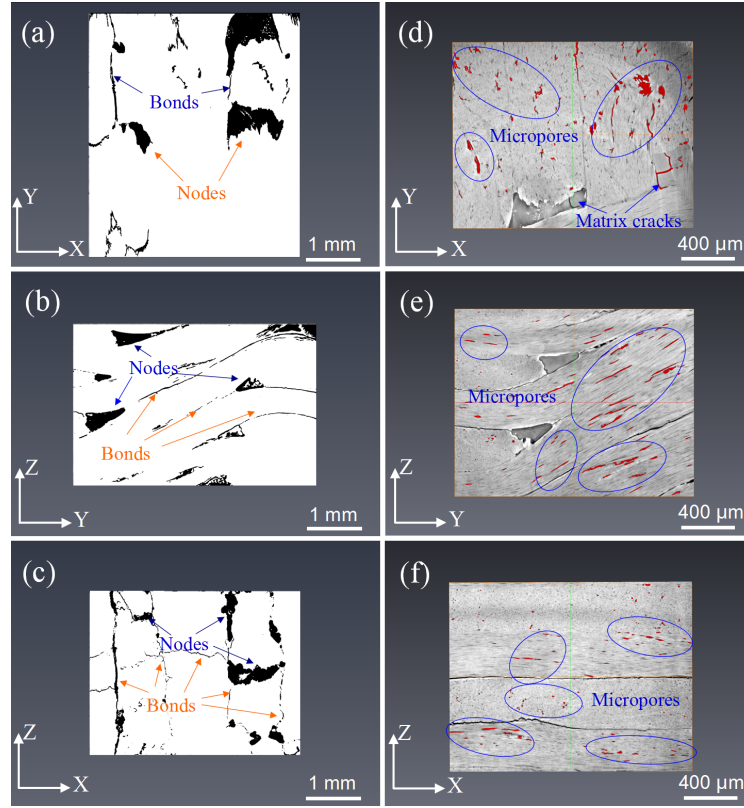


Fig. 3 Segmentation of (a-c) inter-fiber bundle open pores and (d-f) intra-fiber bundle close pores

4.2 3D pore morphology and porosity analysis

It is known that different fiber architectures would exhibit different resistances to composite densification and result in different pore morphology [14]. So it is necessary to have a better understand of the actual 3D porosity shape. Fig. 4 shows the 3D volume rendering of the pores within the 2.5D SiNO₂/BN composite, containing both the open and close pores. The reinforcing fibers and BN matrix are made transparent so as to display the interconnected networks of the pores. It can be seen that the interconnected networks are mainly composed of large open pores with irregular shape. In comparison, the close micropores are isolated from the networks and are mostly piping in shape. By labeling analysis of the different pores, the pore volume of each pore can be obtained (Fig. 4c). The porosity of the composite is then calculated by the whole volume of all pores dividing by the total size of the specimen, which is approximately 8.9%.

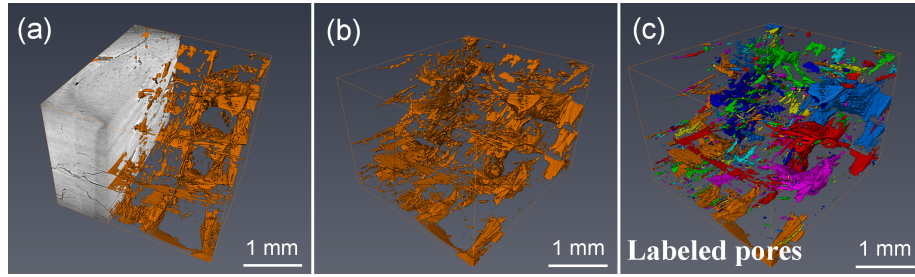


Fig. 4 Renconstruction of 3D pore morphology in the 2.5D SiNO₂/BN composite (a) with fiber and matrix, (b) without fiber and matrix, (c) labeled pores

By filtering the size of the pores, it is also possible to estimate the closed porosity relative to the whole porosity. This has been carried out by applying a “filtering analysis” module in Avizo software, which allows one to select the filtered pores by setting thresholds to specific parameters; the pore volume3d is used in the present study. Fig. 5 shows the influence of threshold value on the content of the chosen pores (sum of those pores having lower volume than the threshold value) against the total porosity. There are four interested volume3d intervals investigated. To have a clear vision of the pore structure, the 3D morphology of the filtered pores in each interval has also been screened out. In interval I, only isolated micropores are presented. The associated volume3d histogram in Fig. 6 suggests that most of the micropores are at a very small size, with a median volume size of $397793.2 \mu\text{m}^3$. This corresponds to a length of $316.7 \mu\text{m}$ for a piping shape pore with a diameter twice of the fiber ($20 \mu\text{m}$). The calculated size agrees well with the segmentation result shown in Fig. 3. As the threshold value increases, larger pores appear in interval II. However, since some of these pores are connected to the specimen surface, it would be slightly overestimated to take all these pores as close pores. When the threshold value is larger than $3250000 \mu\text{m}^3$ (interval III and IV), evident large open pores become included in the filtered pores. It can therefore be concluded that the close porosity level is about 7.1~9.3 % of the total porosity. The calculated open porosity is thus approximately 8.0 to 8.3 % of the observed volume, which is in good agreement with the 7.5 % open porosity of a much larger volume, measured by the Archimedes method; some heterogeneity of porosity is to be expected.

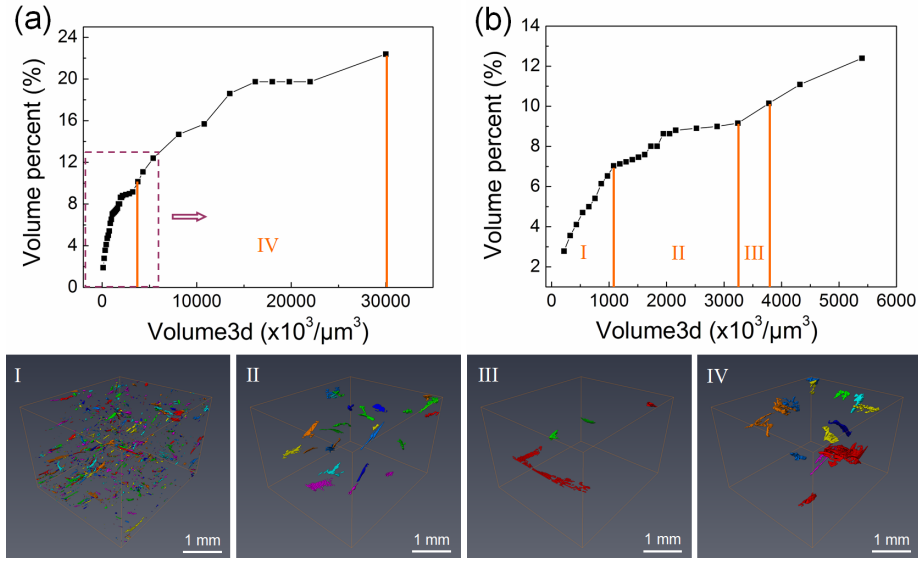


Fig. 5 The volume percent of the filtered pores that displaying lower volume size than the threshold value against the total porosity by applying volume3d filtering analysis, and the corresponded 3D morphology of the filtered pores.

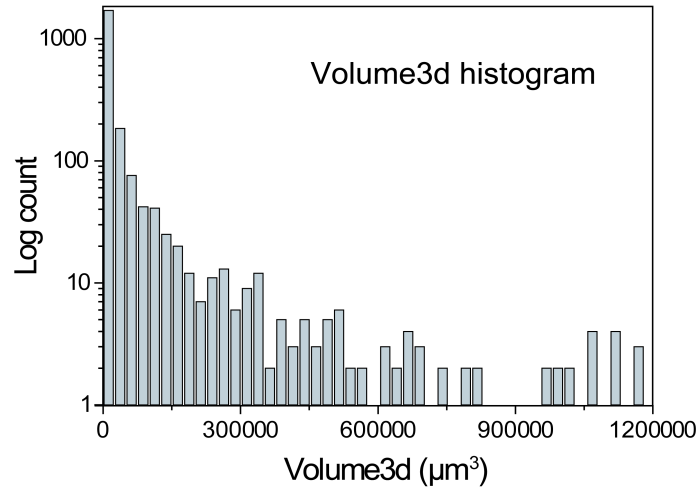


Fig. 6 Volume3d histogram of the micropores whose volume is lower than 1200000 μm^3

5. Conclusions

High-resolution synchrotron X-ray computed tomography (XCT) has been used for characterizing the pore structure and porosity of 2.5D SiNO_f/BN composite, which is essential for understanding the desiccation process and the porosity-related strength deterioration. The results demonstrate the ability of XCT to resolve different scaled pores between inter-bundles and within individual intra-bundles. The 3D volume rendering of the pores provides direct view of the 3D morphology and their connectivity. By filtering analysis of the labeled pores, the total porosity of the observed section of composite is calculated to be 8.9 %, and the closed porosity relative to the total porosity is about 7.1~9.3 % .

Acknowledgments

This work was carried out with the support of the National Natural Science Foundation of China (No. 51302314), Aid Program for Science and Technology Innovation Research Team in Higher Educational Institution of Hunan Province and Aid Program for Innovative Group of National University of Defense Technology and China Scholarship Council (No.201306110050) and the UK EPSRC project “QUBE: Quasi-Brittle fracture: a 3D Experimentally-validated approach” (EP/J019992/1), TJM gratefully acknowledge the support of Oxford Martin School. Access to the I12 Imaging Beamline at the Diamond Light Source as part of experiment EE9036 is gratefully acknowledged, as is the assistance of Dr N. Vo with the image reconstruction.

References

- [1] R. Naslain, *Design, preparation and properties of non-oxide CMCs for application in engines and nuclear reactors: an overview*, *Compos. Sci. Technol.* **64** (2004)155-70.
- [2] M. Takeda, et al., *Strength of a Hi-Nicalon™/silicon-carbide-matrix composite fabricated by the multiple polymer infiltration-pyrolysis process*, *J. Am. Ceram. Soc.* **82** (1999)1579-1581.
- [3] A. Morales-Rodriguez, et al., *Porosity analysis of long-fiber-reinforced ceramic matrix composites using X-ray tomography*, *Scripta. Mater.* **60** (2009)388-90.
- [4] J.H. Shaw, et al. *Effects of tow-scale holes on the mechanical performance of a 3D woven C/SiC composite*, *J. Am. Ceram. Soc.* **98** (2015)948-956.
- [5] L.S. Mora, et al., *3D cellular automata finite element (CAFE) modelling and experimental observation of damage in quasi-brittle nuclear materials: Indentation of a SiC-SiC fibre ceramic matrix composite*, in *3rd International Workshop on Structural Materials for Innovative Nuclear Systems (SMINS-3)*, 2013. October, 2013, Idaho Falls, USA.
- [6] E. Weber, et al., *Comparison of X-ray microtomography measurements of densities and porosity principally to values measured by mercury porosimetry for carbon-carbon composites*, *Carbon* **48** (2010)2151-8.
- [7] E. Maire, et al., *Quantitative X-ray tomography*, *Int. Mater. Rev.* **59** (2014)1-43.
- [8] M. Herbig, et al., *3-D growth of a short fatigue crack within a polycrystalline microstructure studied using combined diffraction and phase-contrast X-ray tomography*, *Acta. Mater.* **59** (2011)590-601.
- [9] C. Zou, et al., *Fabrication and properties of borazine derived boron nitride matrix wave-transparent composites reinforced by 2.5 dimensional fabric of Si-N-O fibers*, *Mater. Sci. Eng.: A* **620** (2015)420-427.
- [10] S. Titarenko, et al., *An analytical formula for ring artefact suppression in X-ray tomography*, *Appl. Math. Lett.* **23** (2010) 1489-1495.
- [11] S. Zhao, et al., *Fabrication and characterization of 2.5D and 3D SiC_f/SiC composites*, *Fusion Eng. Des.* **88** (2013)2453-2456.
- [12] T.L. Starr., *Gas transport model for chemical vapor infiltration*, *J. Mater. Res.* **10** (1995)2360-6.

- [13] X.Wei, et al., *Numerical simulation for fabrication of C/SiC composites in isothermal CVI reactor*, *Comp. Mater. Sci.* **38** (2006)245–55.
- [14] Y. Feng, et al., *Micro-CT characterization on porosity structure of 3D C_f/SiCm composite*, *Compos. Part A: Appl. Sci. Manufact.* **42** (2011)1645-1650.